Continuous Recording and Stochastic Analysis of PD

P. von Glahn and R. J. Van Brunt

National Institute of Standards and Technology,
Gaithersburg, MD

ABSTRACT

We describe the design and use of a digital partial discharge (PD) data recording system capable of continuous real-time recording of PD pulse trains. The recording system consists of a custom two-channel PD digitizer coupled to a personal computer via a 16-bit parallel interface. The digitizer is under software control with the resulting data being stored in binary files on the computer's hard disk. The stored data subsequently are subjected to stochastic analysis using appropriate computer software. Because all data are retained and the computer provides the desired stochastic analysis of data files, the new system is well suited to investigate non-stationary PD behavior such as encountered in aging studies. By way of illustration, the new system was used to determine the time-varying stochastic behavior of ac-generated PD from point-to-dielectric gaps in air where the insulation material was cast epoxy with aluminum oxide filler. The results confirm and extend previous measurements made with an analog stochastic analyzer. With these sample results, we demonstrate how the system allows detailed stochastic analyzes not possible with data obtained from existing conventional PD measurement systems.

1. INTRODUCTION

WITH the advent of high-speed digital logic and computers, it was natural to apply these to the measurement of partial discharge (PD) signals. By the mid 1970's, a number of authors had reported using digital processors to acquire and process PD signals in real time, mostly for pulse-height analysis [1–3]. By the late 1980's, computer processing of PD data to determine phase-resolved PD signatures had supplanted the earlier analysis techniques [4–7]. Coupling a high-speed personal computer with a custom digital data acquisition system for real-time recording and post-test PD analysis using both phase-resolved PD signatures and neural networks was a logical next step in the development of digital PD analysis technology [8–10].

In the early 1990's, Van Brunt recognized that PD is often a complex, non-Markovian point process, requiring sophisticated stochastic analyzes to understand the physical basis for the statistical nature of the phenomenon [11]. This led to the development of a real-time analog PD stochastic analyzer [12] that allowed direct measurement of various conditional PD phase and amplitude distributions. These measurements make possible a complete stochastic characterization of PD that can, for example, reveal detailed information about memory propagation. The analog analyzer, however, relies on a limited number of multichannel analyzers (one per distribution being measured), and therefore the number of distributions that can be determined simultaneously by this analyzer is severely limited. Moreover, it does not make efficient use of the available information since it 'filters' the data as received and does not provide a complete, permanent record of all PD events during the time of observation. This is a serious limitation, characteris-

1070–9878/95/ $3.00

tic of most other PD measurement systems such as those yielding phase-resolved pulse-height distributions.

To remedy these limitations, we designed the PD digitizer-recorder described here that generates a record of *all* PD events in a given time interval. The digitizer interfaces directly to a personal computer to allow continuous recording of PD signals in real time and a subsequent complete stochastic analysis of the recorded data [13]. From the recorded data, a complete history of PD activity can be reconstructed for a particular test or experiment. To illustrate these analyzes, we present data on the stochastic properties of PD during short-term ($\sim$ 2000 s) PD-induced aging of epoxy for point-epoxy gaps. The results are consistent with and extend those previously reported [14, 15] wherein the data were obtained from the less efficient analog stochastic analyzer mentioned above.

In the following Section, we briefly describe the architecture and operation of the new digitization and recording systems. After a description of the experimental configuration and procedure, we present the results of different types of stochastic analyzes which yield detailed statistical information needed to reveal, for example, pulse-to-pulse or phase-to-phase correlations and memory effects that characterize discharge behavior.

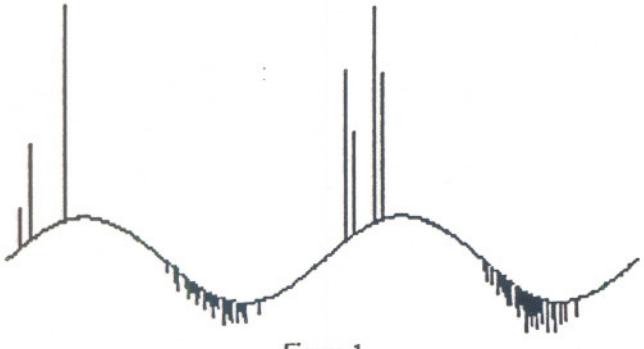

Figure 1.

Sample PD signal for two successive, randomly selected cycles of applied voltage.

2. DIGITIZER DESCRIPTION

The NIST PD recording system (PDRS) consists of two parts: a digitizer and an interface card installed in a personal computer (PC). The PDRS digitizes a PD pulse stream as a series of 16-bit words that are stored as a binary file on the PC's hard disk. The polarity, amplitude, and time since the last positive-going zero-crossing of the applied alternating voltage are recorded for each pulse according to the format defined in Table 1. A word indicating the beginning of a cycle (*i.e.*, the positive-going zero crossing) is also recorded. A 5-bit record number included within the amplitude and zero-crossing words allows multiple records to be stored within one data file.

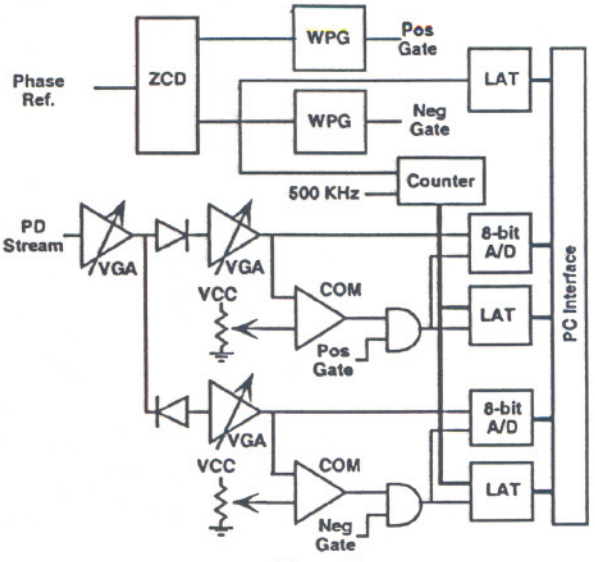

Figure 2.

PD digitizer block diagram. A/D: Analog to digital converter, COM: Analog voltage comparator, LAT: Digital latch, PR: Precision rectifier, VGA: Variable gain amplifier, WPG: Window pulse generator, ZCD: Zero crossing detector.

To illustrate the exact format used, Figure 1 shows two consecutive, randomly selected, cycles of PD data that were reconstructed from the digitized information given in Table 2.

The digitizer, shown in Figure 2, is similar to that reported by other investigators [9, 10]. It is connected to a custom 16-bit interface card in the PC (not shown). The custom interface provides rate buffering and temporary storage of digitizer data prior to processing by the PC. The digitizer is under the control of software running on the PC and consists of two sections: a timing generator and a two-channel digitizer.

The timing generator section is based on a phase reference signal derived from the ac excitation source by external circuitry. A zero-crossing detector generates pulses at both the negative-to-positive and positive-to-negative zero-crossings of a reference signal derived from the applied voltage. The negative-to-positive zero-crossing pulse causes transfer of a cycle start word to the PC. It also resets the pulse time counter and triggers a variable window pulse generator that generates a gate for negative PD pulses. The positive-to-negative pulse likewise triggers a second window pulse generator to provide a gate for positive PD pulses Because PD pulses associated with the positive (negative) excitation half cycle can occur prior to the negative-to-positive (positive-to-negative) zero crossing of the excitation waveform, the window for positive (negative) PD pulses must be triggered by the preceding

Table 1. Digitizer recorded data format in binary and hexadecimal notation.

Hexadecimal	Binary	Meaning
0*raa* – 1*raa*	000*rrrrr aaaaaaaa*	Positive Pulse Amplitude
2*raa* – 3*raa*	001*rrrrr aaaaaaaa*	Negative Pulse Amplitude
4*ppp* – 5*ppp*	010*ppppp ppppppppp*	Phase
6*rxx* – 7*rxx*	011*rrrrr xxxxxxxx*	Zero-crossing Marker
Notation: *rrrrr*: 5-bit record number; *a...a*: 8-bit pulse amplitude; *p...p*: 13-bit pulse phase; *x...x*: random data.		

Table 2.

Sample digitizer data corresponding to Figure 1 in hexadecimal notation. First column is address within data file. Zero-crossings underlined.

000100 :	440*c*	2108	61*ff*	403*c*	0112	4065	0134	40*f*3
000110 :	0174	4282	2109	4296	2115	42*a*8	2128	42*c*7
000120 :	210*e*	42*d*3	2124	42*de*	210*c*	42*e*9	210*c*	42*f*4
000130 :	2121	42*ff*	210*c*	430*b*	210*e*	4310	2122	431*c*
000140 :	210*a*	4326	2112	4332	212*a*	433*b*	2109	4344
000150 :	2113	4355	2135	435*e*	2118	4370	2121	437*e*
000160 :	2127	438*d*	2126	4395	210*b*	43*a*5	2116	43*ad*
000170 :	2122	43*df*	2113	61*ff*	405*c*	013*b*	4078	0123
000180 :	40*c*9	014*c*	40*ed*	0133	4277	2105	4287	210*e*
000190 :	429*a*	210*f*	42*ad*	211*b*	42*b*7	2108	42*c*5	210*a*
0001*a*0 :	42*ca*	2116	42*da*	211*b*	42*e*5	211*b*	42*f*8	211*a*
0001*b*0 :	4300	2122	430*d*	210*e*	4316	2112	4320	2136
0001*c*0 :	432*c*	2118	4338	2128	4341	2115	4350	212*a*
0001*d*0 :	4357	210*c*	4367	211*a*	4375	211*f*	437*c*	212*a*
0001*e*0 :	438*e*	210*e*	4399	2125	43*b*0	2116	43*c*4	2114
0001*f*0 :	43*ec*	210*c*	61*ff*	4059	0139	40*ac*	0157	40*d*7

zero crossing pulse. The two window pulse generators are manually adjusted so that the gates cover the phase range where positive (negative) pulses are observed. Note that PD pulses immediately prior to the negative-to-positive zero-crossing will be stored with the previous cycle. In the subsequent data analysis, these pulses are automatically identified with the correct cycle.

The digitizer section is preceded by an analog signal conditioner. The analog conditioner accepts a stream of bipolar PD pulses from a preamplifier and PD current sensing impedance. For our application, we used a purely resistive sensing impedance on the ground side of discharge gap [16]. The voltage generated by the sensing impedance is capacitively coupled to a preamplifier that amplifies and broadens the pulses to 1.5 μs halfwidth. The preamplifier has a bandpass response between 4.6 and 360 kHz (−3 dB) with third-order high-pass and first-order low-pass rolloff. This preamplifier is identical to that used in our previously-published work [13–16, 19]. Possible errors associated with the use of this amplification scheme have also been discussed previously [12].

After an initial amplification in the PDRS, the PD stream is fed to a pair of precision rectifiers (half-wave rectifiers implemented with operational amplifiers and diodes) to separate the stream into separate positive and negative pulse streams. Further amplification follows to bring the pulses within the range of the analog-to-digital (A/D) converters. Separate amplification is provided for each pulse polarity to insure maximum usable dynamic range when digitizing PD pulses generated under asymmetric discharge gap conditions in which differences between positive and negative pulse amplitudes of a factor of 10 is not uncommon. The bandwidth of these analog amplifiers is sufficient to preserve the preamplifier output waveform as observed on an oscilloscope. The digitizer part consists of two identical circuits, one for each pulse polarity. The PD pulse is digitized by an 8-bit peak-detecting A/D converter that stores the largest input amplitude detected while it is enabled. The PD pulses are also fed to a voltage comparator. When the pulse amplitude exceeds a variable voltage threshold, the comparator output becomes active. If the PD pulse falls within the window generated by the pulse generator, the comparator output triggers storage of the current value of the pulse time counter. Since the time counter is clocked by a 500 kHz signal, the time resolution of the digitizer

is 2 μs, corresponding to $2.4\times10^{-4}\pi$ rad at 60 Hz. The comparator output is also used to disable the A/D converter after a delay sufficient to allow the PD signal to reach its peak value. The delay time can be adjusted between 0.5 and 2 μs to match the pulse width delivered by the preamplifier. Note that this width is also a function of the PD source geometry, gas pressure and composition, and PD excitation voltage, so the delay time may have to be changed for different PD source conditions. After the A/D converter is disabled, the amplitude and phase data are transferred to the PC for recording. Since the transfer process is completed in 1.5 μs, the minimum inter-pulse resolution time of the instrument is 1.5 μs longer than the delay setting (2.5 μs for the configuration used in this paper). After the data are transferred, the A/D converter is enabled for the next PD pulse.

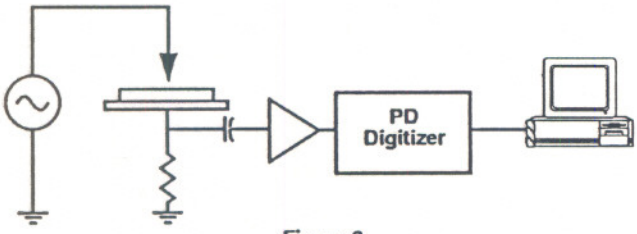

Figure 3.
Experimental configuration block diagram.

3. EXPERIMENTAL PROCEDURE

As an illustration of the capabilities provided by the new digitizer, we present results obtained using the system described above to record PD from a point-plane geometry. We used a stainless steel point electrode displaced from a flat epoxy dielectric sample in room air as previously described [13–16] and shown in Figure 3. For a given set of experimental conditions, we adjusted the input amplifiers to keep the PD signals within the range of the A/D converter. The A/D trigger comparator thresholds were also manually adjusted by simultaneously observing the signal latching the pulse time counter and the signal at each A/D input with an oscilloscope.

As in our previous work, we performed each 'aging' experiment using a different, widely separated location of the point electrode on an 8×8 cm^2 epoxy sample. As previously reported [16], when power was initially applied to the needle, PD pulses appeared on both the positive and negative half cycles. The PD-induced increase in the dielectric surface conductivity eventually causes cessation of PD pulses on the positive half cycles, particularly when the point touches the epoxy surface [16]. For the tests reported here, we continued data acquisition until well after positive pulse cessation time as determined by monitoring the PD signals with an oscilloscope.

After the data were collected, we calibrated the digitizer amplifiers using a pulse signal applied to a known capacitor connected in place of the point-plane gap shown in Figure 3. The calibration is used to obtain a relationship between pulse amplitude and PD charge in pC as discussed previously [12,23]. Stochastic analysis of the stored PD data was subsequently performed with custom software. Examples of results from the stochastic analysis process are shown below.

4. DEFINITIONS

In what follows, the charge on the nth positive pulse (in pC) is represented by q_n^+, the phase-of-occurrence of the pulse (in radians) by ϕ_n^+, and the integrated charge on the positive half cycle (also in pC) by $Q^+ = \sum_n q_n^+$. Likewise, q_n^-, ϕ_n^-, and $Q^- = \sum_n q_n^-$ refer to the corresponding quantities associated with the nth negative pulse. Since PD is a stochastic phenomenon in which memory effects may be important, a complete stochastic description requires both conditional and unconditional probability distributions such as $p_1\left(\phi_1^- \,|Q^+\right)$ which gives the probability that the phase of the first negative pulse is between ϕ_1^- and $\phi_1^- + d\phi_1^-$ when the positive integrated charge on the previous half cycle is restricted to a particular value or range of values [12]. Many other types of conditional distributions can be determined from the data as illustrated below. These distributions can be used to extract information about pulse-to-pulse correlations and memory propagation [19,21].

5. EXPERIMENTAL RESULTS

As an illustration of the capabilities provided by the new digitizer, we present examples of detailed stochastic information derived from data acquired using the system described above to continuously record PD from a point-dielectric gap. Epidian Type 2 Epoxy™ with Al_2O_3 filler was used as the dielectric. A sinusoidal excitation (V_{rms} = 3 kV, f = 200 or 400 Hz) was used with a 330 Ω PD current sensing resistor. Two different experimental configurations were used to collect the data reported here, namely a gap of 0 mm with 400 Hz excitation and a gap of 0.5 mm with 200 Hz excitation. For the first configuration, PD was primarily due to surface discharge while for the second it was due to a combination of gaseous and surface discharge. We collected two data files during separate aging experiments, one for each configuration. The resulting data files occupied 24 MB disk space for the first configuration and 27.3 MB for the second.

Short-term PD-induced aging of epoxy has been studied previously in our laboratory [13–16]. The observed nonstationary behavior of PD during aging was found to

result from a PD-induced increase in the surface conductivity of the dielectric. It has been shown that this increase is associated primarily with acidic deposits during the discharge [17]. For our purposes, aging is manifested by changes to the stochastic properties of the PD pulses as discussed below.

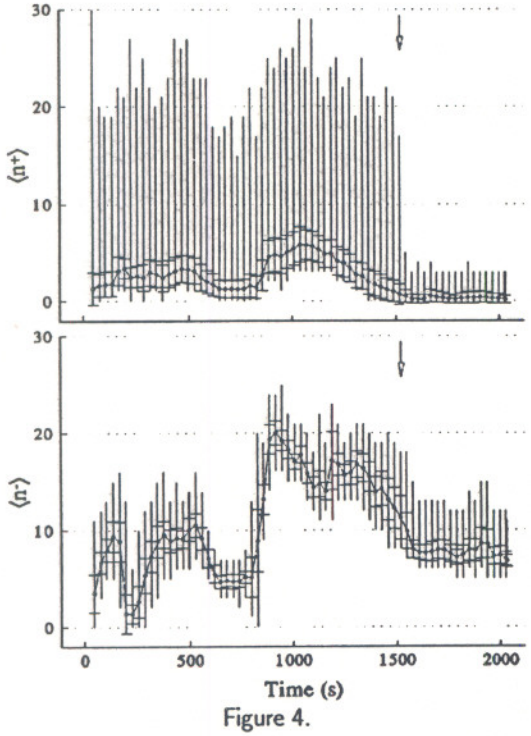

Figure 4.

Mean number of positive $\langle n^+ \rangle$ and negative $\langle n^- \rangle$ pulses per cycle *vs.* time. Vertical bars connect extrema. Error bars indicate one standard deviation from the mean. Arrow indicates time of 'cessation' of positive pulses. $d = 0$ mm, 400 Hz, 30 s processing period.

5.1. SURFACE DISCHARGE ($d = 0$ mm)

We consider first the configuration with the point touching the insulator. In this case, the PD phenomenon is primarily governed by the dielectric surface since there is essentially no gas between the tip of the electrode and the dielectric surface. An overview of the effect of aging on PD behavior is obtained by examining the time dependence of the mean number of positive ($\langle n^+ \rangle$) and negative ($\langle n^- \rangle$) PD pulses per cycle as shown in Figure 4. We generated these plots by determining the average, standard deviation, and maximum and minimum of the number of pulses on a cycle during consecutive blocks of 12000 cycles (30 s). The maxima and minima are plotted as vertical bars, the standard deviations as error bars, and the average values as a set of connected dots. Note that the positive pulses essentially cease at approximately 1520 s from power application as marked by the vertical arrow. Note also that cycles with no positive pulses occur well before this 'cessation'. After this time, there are occasional cycles in which one or more positive PD pulses occur. The near disappearance of positive PD is consistent with earlier observations [14, 15]. It is also consistent with predictions made by Van Brunt and coworkers using a Monte Carlo simulation that models the behavior of PD as a function of changes in surface conductivity [16, 18].

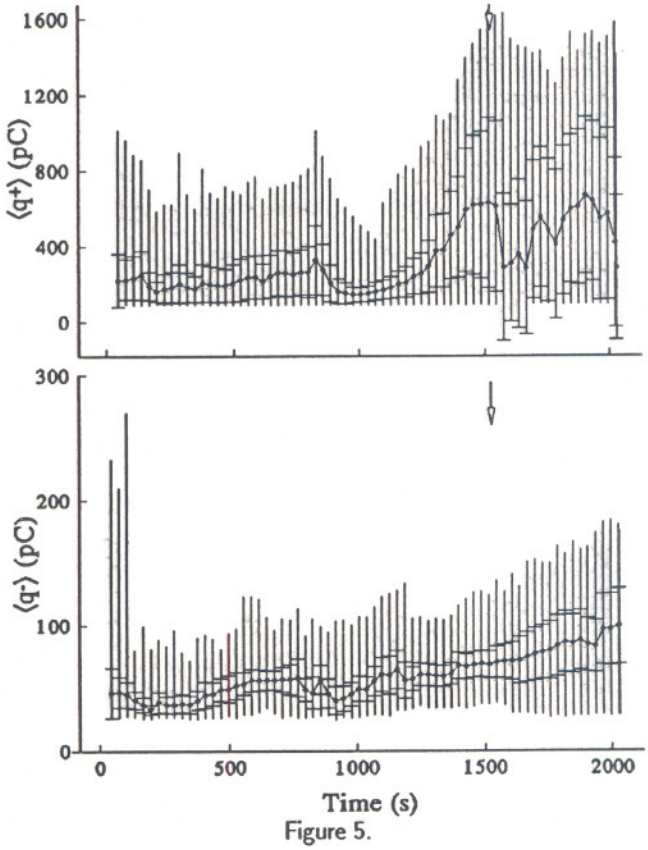

Figure 5.

Mean positive $\langle q^+ \rangle$ and negative $\langle q^- \rangle$ pulse amplitude per cycle vs. time. Vertical bars connect extrema. Error bars indicate one standard deviation from the mean. Arrow indicates time of 'cessation' of positive pulses. $d = 0$ mm, 400 Hz, 30 s processing period.

While the average number of positive pulses drops dramatically as the epoxy ages, the few pulses that do occur after 1520 s are of significantly higher amplitude as seen in Figure 5. Figure 5 shows the mean amplitudes of positive and negative pulses ($\langle q^+ \rangle$, $\langle q^- \rangle$) per cycle together with their extrema and standard deviations *vs.* time. While the number of negative pulses tends to stabilize after 1520 s to $\sim$ 8 pulses per cycle, the average amplitude and statistical variability of the negative pulses increase, suggesting the onset of another slower aging process. As shown previously [16], we can gain additional

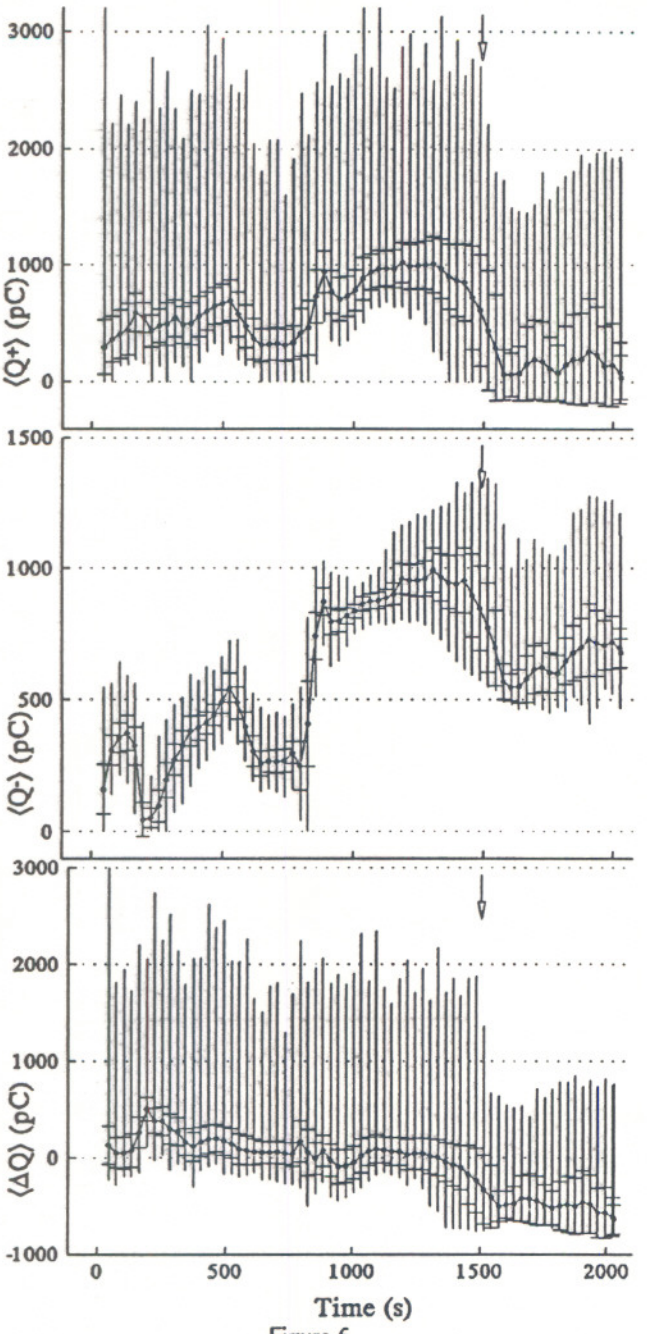

Figure 6.

Mean positive, negative, and net integrated charge per cycle *vs.* time. Vertical bars connect extrema. Error bars indicate one standard deviation from the mean. Arrow indicates time of 'cessation' of positive pulses. $d = 0$ mm, 400 Hz, 30 s processing period.

insight into the effects of the aging process by examining the mean values of positive and negative integrated charge ($\langle Q^+ \rangle$, $\langle Q^- \rangle$) as well as of the mean net charge difference

$$\langle \Delta Q \rangle = \left\langle \left| \sum_n q_n^+ \right| - \left| \sum_n q_n^- \right| \right\rangle \qquad (1)$$

per cycle as shown in Figure 6. In this case, the net charge per cycle is calculated on a cycle-by-cycle basis by subtracting the absolute value of the total negative-pulse amplitude from the total positive-pulse amplitude. The behavior of the net charge indicates that, in order to maintain charge balance ($\langle Q^+ \rangle \cong \langle Q^- \rangle$) after 1520 s, a charge flow not associated with PD pulses must exist to counterbalance the net excess negative impulsive charge. Also note that for every 30 s processing period, at least one cycle occurs in which the mean PD charge per cycle differs substantially from zero, indicating that absolute charge balance does not occur for every cycle.

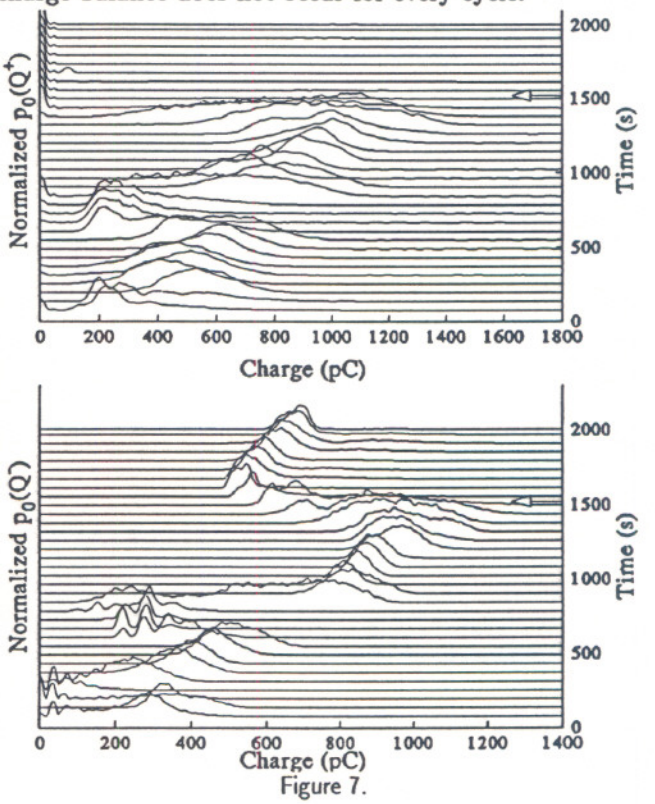

Figure 7.

Time sequential normalized positive and negative pulse integrated charge per cycle. Arrow indicates time of 'cessation' of positive pulses. $d = 0$ mm, 400 Hz, 60 s processing period.

While these plots give the trend for mean integrated charge, we can obtain additional insight into the time varying nature of this quantity by observing the unconditional distributions of positive and negative integrated charge ($p_0(Q^+), p_0(Q^-)$) presented in Figure 7. These give a more refined view of the likelihood that a particular level of integrated charge will occur at a given instant. We arbitrarily normalized the distributions shown

in Figure 7 to the maximum value to display all the distributions on the same scale.

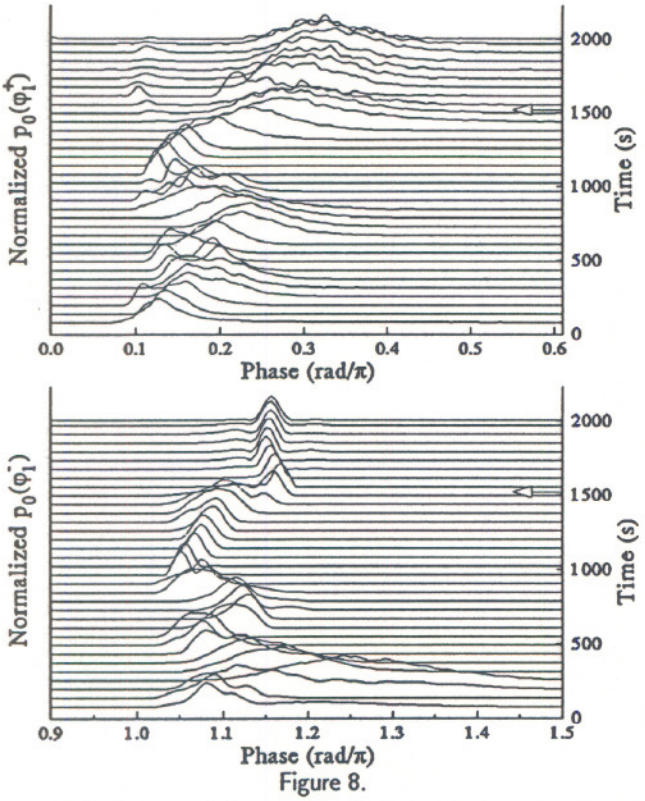

Figure 8.

Time sequential normalized phase-of-occurrence of the first positive and negative pulse on a cycle. Arrow indicates time of 'cessation' of positive pulses. $d = 0$ mm, 400 Hz, 60 s processing period.

The phase-of-occurrence of a given pulse also changes as the integrated charge changes since the phase and integrated charge are not independent quantities but rather are related by integral expressions [12, 16, 19]. Specifically, the distribution in phase of the first positive PD pulse ϕ_1^+ is related to the negative integrated charge distribution on the previous half cycle by

$$p_0(\phi_1^+) = \int_0^\infty p_0(Q^-)\, p_1(\phi_1^+ | Q^-)\, dQ^- \qquad (2)$$

and similarly the phase of the first negative pulse, ϕ_1^-, is related to the positive integrated charge on the previous half cycle by

$$p_0(\phi_1^-) = \int_0^\infty p_0(Q^+)\, p_1(\phi_1^- | Q^+)\, dQ^+ \qquad (3)$$

Similar relationships apply to the phases of subsequent pulses [19]. Figure 8 presents a time sequential view of the unconditional phase distributions given by Equations (2) and (3). The virtual disappearance of positive pulses at 1520 s results in a shift of the first negative pulse toward the negative half cycle maximum as reported in our earlier work [16]. The infrequent positive pulses that do occur after this time tend to appear at $\sim 0.3\pi$ rad at a time on the positive half cycle where the rate of change of the voltage is lowest. We emphasize again that these distributions have been normalized to the maxima and therefore do not indicate the absolute probability of occurrence per cycle.

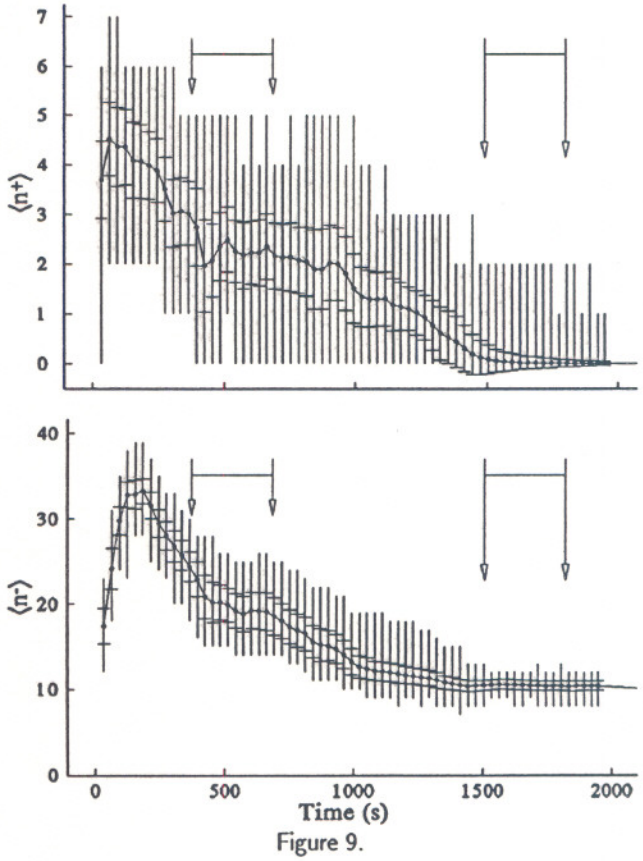

Figure 9.

Mean number of negative and positive pulses per cycle vs. time. Vertical bars connect extrema. Error bars indicate one standard deviation from the mean. Arrow pairs connected by line indicates time periods represented by Figures 11 to 16 and Figures 17 and 18. $d = 0.5$ mm, 200 Hz, 30 s processing period.

5.2. SURFACE AND AIR DISCHARGE ($d = 0.5$ mm)

In a previous work [20], we noted that the characteristics of PD changes dramatically with the introduction of a small point-to-dielectric gap. In the case of polytetrafluoroethylene (PTFE) dielectric, the most dramatic changes occur as the spacing is increased from 0 to 2.5 mm. The following results were obtained in air with

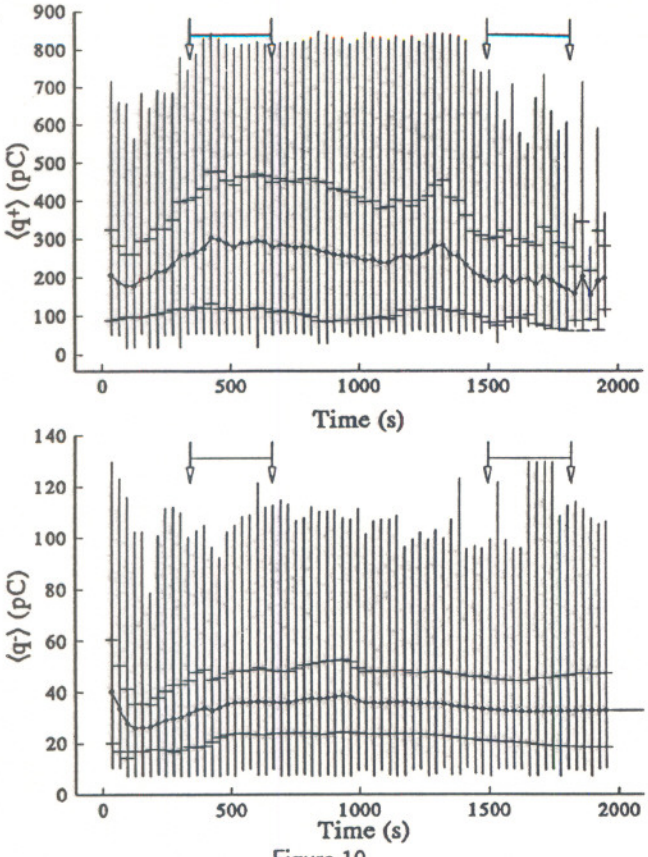

Figure 10.

Mean negative and positive pulse amplitude *vs.* time. Vertical bars connect extrema. Error bars indicate one standard deviation from the mean. Arrow pairs connected by line indicates time periods represented by Figures 11 to 16 and Figures 17 and 18. $d = 0.5$ mm, 200 Hz, 30 s processing period.

a very small (0.5 mm) gap. As can be seen from Figure 9, the number of pulses *vs.* time follows the same general pattern as for a 0 mm gap (Figure 4), that is, an initial period of conditioning (in this case, $\sim$ 150 s) followed by a gradual decline with the positive pulses essentially ceasing at $\sim$ 1500 s. The number of positive pulses is noticeably smaller and the number of negative pulses considerably larger than for the $d = 0$ case. Furthermore, prior to the cessation of the positive PD more cycles with no positive pulses occur than when no air gap exists.

As seen from the average amplitude of the pulses shown in Figure 10, the amount of variability with time of both the positive and negative amplitudes is less than that for $d = 0$ (compare with Figure 5). Also, the average negative-pulse amplitude shows no increase after cessation of positive pulses as evident in the case for $d = 0$. We also can use the recorded PD data to generate the usual phase-resolved pulse-amplitude plots generated by conventional PD data acquisition systems performing pulse-height analysis [4–7].

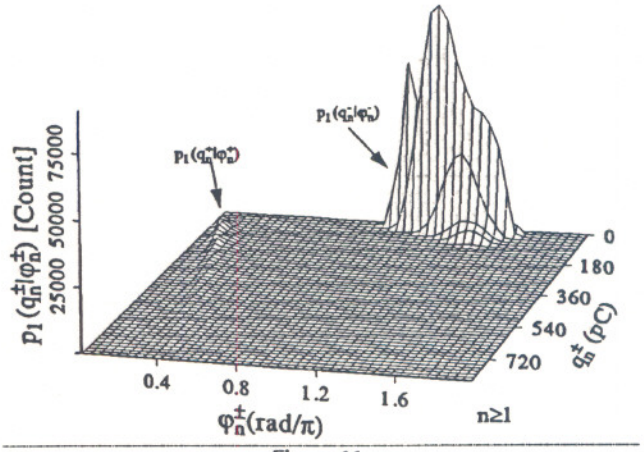

Figure 11.

Unnormalized phase-resolved pulse-amplitude plot. $d = 0.5$ mm, 200 Hz, 400 to 700 s after power application.

An example of such a three-dimensional plot is given in Figure 11. Shown in this Figure are the unnormalized distributions $p_1(q_n^{\pm}|\phi_n^{\pm})$, where $n \geq 1$. $q_n^{\pm}$ are amplitudes contained in the set of intervals $\{q_i + \Delta q\}$ defined by $0 < q_i < 800$ pC, $\Delta q = 16$ pC, and likewise $\phi_n^{\pm} \in \{\phi_i + \Delta\phi\}$, $0 < \phi_i < 2\pi$, $\Delta\phi = 0.045\pi$. Here i is an integer index that specifies a particular amplitude or phase window. While this type of plot produces an interesting pattern that can be compared with the results produced by other PD analyzers, it provides an incomplete indicator of the stochastic characteristics of PD and is very difficult to interpret [16]. In particular, it contains no memory propagation or correlation information and is of limited value in any attempt to understand the underlying physical basis for the observed statistical behavior of the PD phenomenon.

As was reported earlier, the statistical behavior of PD [16,18,19] is governed primarily by memory effects such as associated with charge deposited by PD remaining on a dielectric surface between half cycles. The existence of memory propagation can be revealed by examining the relationship between the total PD charge ($Q^+ or \quad Q^-$) during one half cycle, and the phase distribution of pulses on the subsequent half cycle as discussed previously [20]. If memory is present, there will be a significant correlation between the random variables $Q^{\pm}$ and $\phi_i^{\mp}$. In the present case, the expected relationship exists between the variables as shown in Figure 12 using a three dimensional view of the conditional probability distribution function $p_1(\phi_1^- | Q^+)$ where $\phi_1^- \in \{\phi_i + \Delta\phi\}$, $0.75\pi < \phi_i < 1.25\pi$, $\Delta\phi = 0.01\pi$ and $Q^+ \in \{Q_i + \Delta Q\}$, $0 < Q_i < 1400$ pC, $\Delta Q = 0.11$ pC. A simplified view of the dependence of

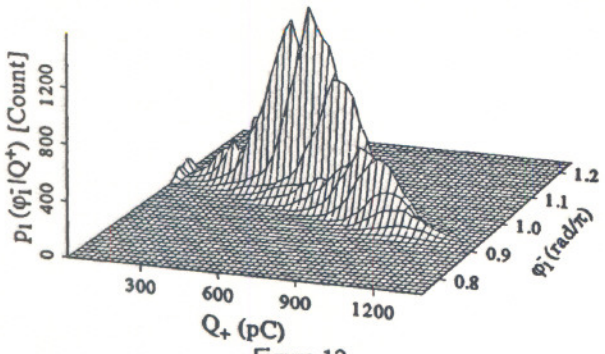

Figure 12.

Not-normalized conditional distribution of phase of first negative pulse conditioned on the positive integrated charge on the previous half cycle, $p_1(\phi_1^- | Q^+)$. $d = 0.5$ mm, 200 Hz, 400 to 700 s after power application.

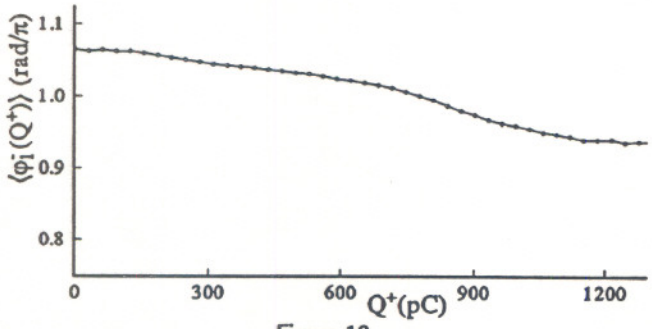

Figure 13.

Mean phase-of-occurrence of first negative pulse as a function of the integrated charge on the previous half cycle. $d = 0.5$ mm, 200 Hz, 400 to 700 s after power application.

ϕ_1^- on Q^+ is shown in Figure 13 in which the expectation value

$$\langle \phi_1^- (Q^+) \rangle = \int_0^{2\pi} \phi_1^- p_1 (\phi_1^- | Q^+) \, d\phi_1^- \qquad (4)$$

is plotted *vs.* Q^+. This plot shows that as Q^+ increases, the mean phase-of-occurrence of the first negative pulse on the next half cycle decreases. This behavior is consistent with previous observations made with an analog stochastic analyzer and predictions from a Monte-Carlo simulation of PD [19].

The PD phenomenon also exhibits pulse-to-pulse memory within a half cycle due to space and surface charges as demonstrated in our earlier work [20]. Figure 14 shows a three-dimensional view of the relation between the amplitude of the second negative pulse and the phase separation between it and the first negative pulse. This corresponds to the conditional distribution $p_1(q_2^- | \Delta\phi_{1,2}^-)$ where $q_2^- \in \{q_i + \Delta q\}$, $0 < q_i < 60$ pC, $\Delta q = 1.33$ pC, and $\Delta\phi_{1,2}^- \in \{\phi_i + \Delta\phi\}$, $0 < \phi_i < 0.1\pi$, $\Delta\phi = 0.002\pi$.

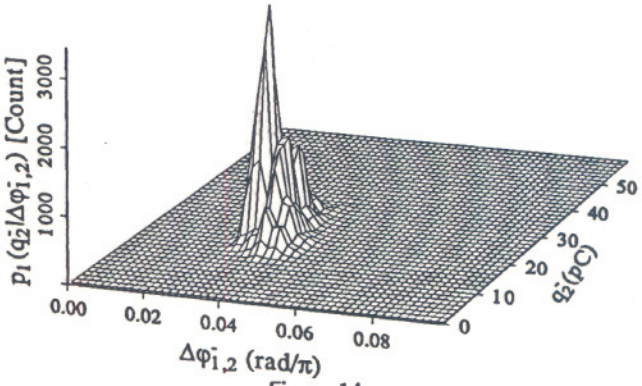

Figure 14.

Not-normalized conditional distribution of amplitude of second negative pulse conditioned on the phase separation from first negative pulse, $p_1(q_2^- | \Delta\phi_{1,2}^-)$. $d = 0.5$ mm, 200 Hz, 400 to 700 s after power application.

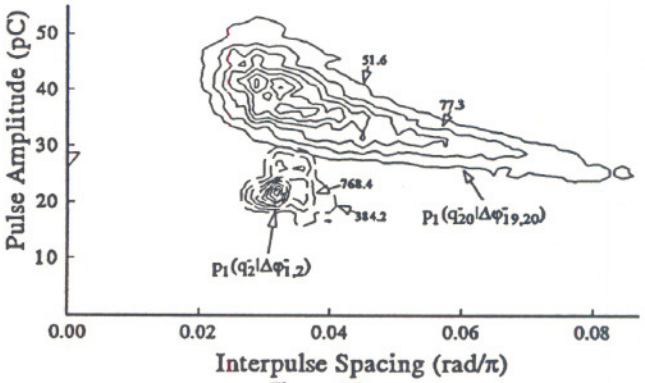

Figure 15.

Not-normalized conditional distribution of amplitude of 20th negative pulse conditioned on the phase separation from 19th negative pulse, $p_1(q_{20}^- | \Delta\phi_{19,20}^-)$. The conditional distribution of amplitude of 2_{nd} negative pulse conditioned on the phase separation from 1_{st} negative pulse, $p_1(q_2^- | \Delta\phi_{1,2}^-)$, is included for comparison. $d = 0.5$ mm, 200 Hz, 400 to 700 s after power application.

A contour plot such as shown in Figure 15 provides another view of the same data. We find that contour plots are more useful than three-dimensional plots for spotting trends in the distribution. As can be seen, the size of the second pulse is not strongly related to the spacing between it and the first negative pulse. Moving later in the negative half cycle, however, we can see from Figure 15 that the size of the twentieth negative pulse exhibits both a larger variability and a noticeable negative dependence between its amplitude and spacing from the previous pulse.

The pulse-to-pulse memory characteristics for positive pulses are somewhat different from those of the nega-

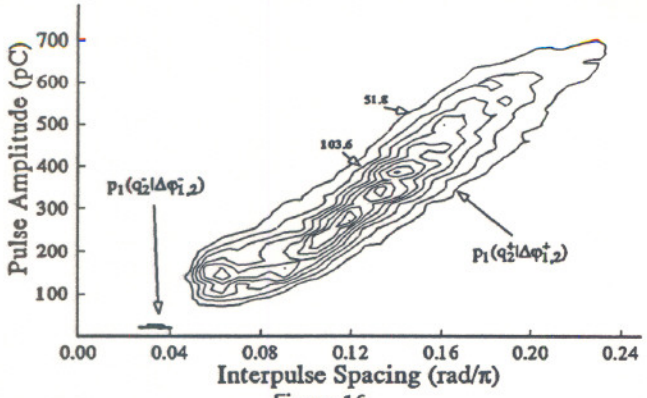

Figure 16.

Not-normalized conditional distribution of amplitude of 2_{nd} positive pulse conditioned on the phase separation from the 1_{st} positive pulse, $p_1(q_2^+|\Delta\phi_{1,2}^+)$. The conditional distribution of amplitude of 2_{nd} negative pulse conditioned on the phase separation from 1_{st} negative pulse, $p_1(q_2^-|\Delta\phi_{1,2}^-)$, is included for comparison. d = 0.5 mm, 200 Hz, 400 to 700 s after power application.

tive pulses. Figure 16 shows a contour plot of the relation between the amplitude of the second positive pulse and the phase separation between it and the first positive pulse. This plot corresponds to $p_1(q_2^+|\Delta\phi_{1,2}^+)$ where $q_2^+ \in \{q_i + \Delta q\}$, $0 < q_i < 800$ pC, $\Delta q = 18.9$ pC, and $\Delta\phi_{1,2}^+ \in \{\phi_i + \Delta\phi\}$, $0 < \phi_i < 0.35\pi$, $\Delta\phi = 0.008\pi$. Unlike the negative pulses, the second positive pulse shows a markedly positive correlation between size and spacing from the first positive pulse. As can be seen by comparing the data for the second negative pulse (reproduced on Figure 16 for comparison), the second positive pulse is also much larger than second negative pulse and separated much further from its predecessor.

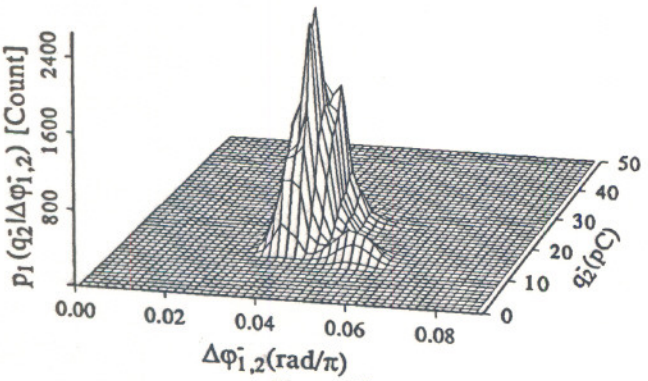

Figure 17.

Not-normalized conditional distribution of amplitude of second negative pulse conditioned on the phase separation from the first negative pulse, $p_1(q_2^-|\Delta\phi_{1,2}^-)$. d = 0.5 mm, 200 Hz, 1500 to 1800 s after power application.

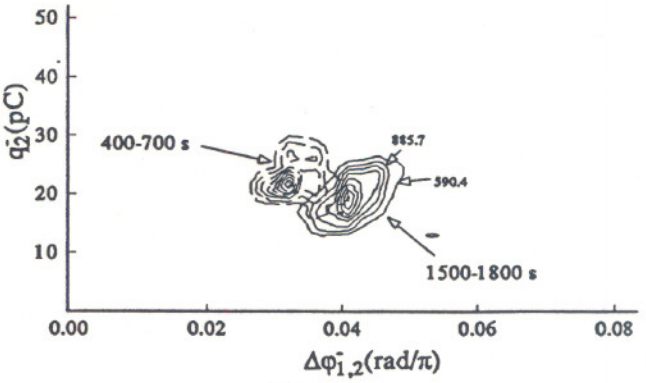

Figure 18.

Not-normalized conditional distribution of amplitude of second negative pulse conditioned on the phase separation from the first negative pulse, $p_1(q_2^-|\Delta\phi_{1,2}^-)$, for two periods after power application. d = 0.5 mm, 200 Hz.

As the insulator ages due to exposure to PD, changes occur in stochastic behavior, *e.g.*, the extent of pulse-to-pulse memory propagation. The previous eight Figures all relate to the same 300 s period relatively early in the aging process (indicated by vertical arrows connected by a horizontal bar in Figures 10 and 11). Turning to a 300 s period beginning at a time after the positive pulses essentially have ceased, we observe that changes have occurred in the relationship between the amplitude of the second negative pulse and its spacing from the first pulse. As an illustration of the changes that occur in the characteristics of the PD during the aging process, Figure 17 gives the same type of data as in Figure 14 but for a 300 s (60000 cycle) period during which the positive PD pulses had ceased. Note the larger mean pulse amplitudes, steeper positive dependence of amplitude on pulse spacing, and the broader spread of pulse-to-pulse spacing compared to the earlier time. The comparison is more obvious in Figure 18 that shows the corresponding contour plots from the two periods.

6. CONCLUSIONS

We have demonstrated that the PDRS provides the ability to record continuously all the information about PD pulse amplitude and phases over extended periods of time. This allows one to review the entire time development of PD and to make new types of analyzes that are impossible with a real-time system, *e.g.*, a system based on pulse-height or phase-resolved pulse-height analysis. Having a complete archival record of the PD data allows multiple analyzes of the same segment of data. Such archival records make possible future data reanalysis based on any new understanding of the PD phenomenon. In addition to obtaining phase-resolved pulse-height information, it is possible also to perform a com-

plete stochastic analysis to look for pulse-to-pulse and/or phase-to-phase correlations indicative of possible memory effects. We have previously shown that the unraveling of such memory effects is *essential* to understanding the underlying physical basis for the stochastic behavior of PD [18–21].

Although the system described here represents a significant advance, it is not without limitations. The present PDRS design is limited to recording PD pulses with an impulsive shape that have a separation of at least 2.5 μs. It may produce incomplete records or inaccurate results for PD streams containing bursts of closely spaced pulses [23,24] or pulses with long 'tails' [25]. It also requires a PC with a fast processor (> 30 MHz) and large hard disk (> 500 MB) to keep up with and store PD pulses. Finally, the current configuration lacks sufficient dynamic range to accurately track PD signals with fluctuations in amplitude that exceed the range of the A/D converter while maintaining calibration.

7. AREAS FOR FUTURE WORK

We plan additional work to further validate the performance of the PDRS through comparison with the analog stochastic analyzer. We will address the dynamic range limitations by adding calibrated, digital gain and threshold settings to replace the current analog controls and allow the system to track signal levels dynamically. Finally, the analysis software is continually being upgraded to take advantage of the new types of analysis made possible by the PDRS so as to gain new understanding into the physics of the PD phenomena and move toward more reliable computerized life predictions of HV apparatus based on PD signals.

ACKNOWLEDGMENT

All measurements were made in the Electricity Division, Electronics and Electrical Engineering Laboratory, National Institute of Standards and Technology, Technology Administration of the U. S. Department of Commerce. Partial support was received from the Division of Engineering, Office of Nuclear Regulatory Research, U. S. Nuclear Regulatory Commission. The epoxy samples used were provided by T. Las of the Electrotechnical Institute, Warsaw, Poland with support from the Maria Sklodowska-Curie Joint Fund, U. S. Polish Joint Commission.

REFERENCES

[1] R. Bartnikas, "Use of a Multichannel Analyzer for Corona Pulse-Height Distribution Measurements on Cables and Other Electrical Apparatus", IEEE Trans. Instr. Meas., Vol. 22. pp. 403–407, 1973.

[2] T. Tanaka and T. Okamoto, "A Minicomputer-Based Partial Discharge Measurement System", Conf. Recd.1978 IEEE Intl. Symp. Elec. Insul., pp. 86–89, Philadelphia, PA, June 12–14, 1978.

[3] J. Austin and R. James, "On-Line Digital Computer Systems for Measurement of Partial Discharges in Insulation Structures", IEEE Trans. Elec. Insul., Vol. 11, pp. 129–139, 1976.

[4] B. Fruth, L. Niemeyer, M. Haessig, J. Fuhr, and Th. Dunz, "Phase Resolved Partial Discharge Measurements and Computer Aided Partial Discharge Analysis Performed on Different High Voltage Apparatus", 6th Intl. Symp. HV Eng., pp. 15.03–15.06, New Orleans, LA, 1989.

[5] M. Hikita, K. Yamada, A. Nakamura, T. Mizutani, A. Oohasi, and M. Ieda, "Measurements of Partial Discharges by Computer and Analysis of Partial Discharge Distribution by the Monte Carlo Method", IEEE Trans. Elec. Insul., Vol. 25, pp. 453–468, 1990.

[6] B. Fruth and D. W. Gross, "Combination of Frequency Spectrum Analysis and Partial Discharge Pattern Recording", Conf. Rec. 1994 IEEE Intl. Symp. Elec. Insul., Pittsburgh, PA, pp. 296–300, June 5–8, 1994.

[7] B. Fruth and L. Niemeyer, "The Importance of Statistical Characteristics of Partial Discharge Data", IEEE Trans. Elec. Insul., Vol. 27, pp. 60–69, 1992.

[8] T. R. Blackburn, B. T. Phung, and R. E. James, "Neural Network Application of PD Pattern Analysis", Conf. Proc. Intl. Conf. Partial Discharge, pp. 82–83, Canterbury, UK, Sept. 28–30, 1993.

[9] C. Hantouche and D. Fortune, "Digital Measurement of Partial Discharges in Full-Sized Power Capacitors", IEEE Trans. Elec. Insul., Vol. 28, pp. 1025–1032, 1993.

[10] R. E. James, B. T. Phung and T. R. Blackburn, "Computer-Aided Digital Techniques for Partial Discharge Measurements and Analysis", Intl. Symp. Digital Techn. High-Volt. Meas., pp. 2.7–2.11, Toronto, Canada, 1991.

[11] R. J. Van Brunt, "Stochastic Properties of Partial Discharge Phenomena", IEEE Trans. Elec. Insul., Vol. 26, pp. 902–948, 1991.

[12] R. J. Van Brunt and E. W. Cernyar, "System for Measuring Conditional Amplitude, Phase, or Time Distributions of Pulsating Phenomena", J. Research of Natl. Inst. Std. Techn., Vol. 97, pp. 634–671, 1992.

[13] P. von Glahn and R. J. Van Brunt, "Performance Evaluation of A New Digital Partial Discharge Recording and Analysis System", Conf. Rec.–1994 IEEE Intl. Symp. Elec. Insul., pp. 12–15, Pittsburgh, PA, June 5–8. 1994.

[14] R. J. Van Brunt, P. von Glahn and T. Las, "Nonstationary Behavior of Partial Discharge During Insulation Aging", Conf. Proc. Intl. Conf. Partial Discharge, pp. 29–30, Canterbury, UK, Sept. 28–30, 1993.

[15] R. J. Van Brunt, P. von Glahn, and T. Las, "Partial Discharge-Induced Aging of Cast Epoxies and Related Nonstationary Behavior of the Discharge Statistics", 1993 Annual Report, Conference on Electrical Insulation and Dielectric Phenomena, pp. 455–461, Pocono Manor, PA, Oct. 17–20, 1993.

[16] R. J. Van Brunt, P. von Glahn, and T. Las, "Nonstationary Behavior of Partial Discharge During Discharge-induced Aging of Dielectrics", IEE Proc.–Sci. Meas. Technol., Vol. 142, pp. 37–45, 1995.

[17] C. Hudon, R. Bartnikas, and M. R. Wertheimer, "Spark-to-glow Discharge Transition due to Increased Surface Conductivity on Epoxy Resin Specimens", IEEE Trans. Elec. Insul., Vol. 28, pp. 1–8, 1993.

[18] R. J. Van Brunt, "Physics and Chemistry of Corona and Partial Discharge – Recent Advances and Future Challenges", IEEE Trans. Diel. and Elec. Insul., Vol. 1, pp. 761–784, 1994.

[19] R. J. Van Brunt, E. W. Cernyar, and P. von Glahn, "Importance of Unraveling Memory Propagation Effects in Interpreting Data on Partial Discharge Statistics", IEEE Trans. Elec. Insul., Vol. 28, pp. 905–916, 1993.

[20] R. J. Van Brunt, P. von Glahn, and T. Las, "Variations in the Stochastic Behavior of Partial-Discharge Pulses with Point-to-dielectric Gap Spacing", Conf. Rec. 1992 IEEE Intl. Symp. Elec. Insul., pp. 349–353, Baltimore, MD, June 7–10, 1992.

[21] R. J. Van Brunt and S. V. Kulkarni, "Stochastic Properties of Trichel-pulse corona: A non-Markovian Random Point Process", Phys. Rev. A, Vol. 42, pp. 4908–4932, 1990.

[22] R. J. Van Brunt, M. Misakian, S. V. Kulkarni, and V. K. Lakdawala, "Influence of a Dielectric Barrier on the Stochastic Behavior of Trichel-Pulse Corona", IEEE Trans. Elec. Insul., Vol. 26, pp. 405–415, 1991.

[23] R. J. Van Brunt and D. Leep, "Characterization of Point-to-Plane Corona Pulses in SF_6", J. Appl. Phys., Vol. 52, pp. 658–600, 1981.

[24] T. V. Blalock, A. L. Wintenberg, and M. O. Pace, "Low-noise Wide-Band Amplification System for Acquiring Prebreakdown Current Pulses in Liquid Dielectrics", IEEE Trans. Elec. Insul., Vol. 24, pp. 641–647, 1989.

[25] R. Bartnikas and J. P. Novak, "On the Character of Different Forms of Partial Discharge and Their Related Terminologies", IEEE Trans. Elec. Insul., Vol. 28, pp. 956–968, 1993.

This paper is based on a presentation given at the 1994 Volta Colloquium on Partial Discharge Measurements, Como, Italy, 31 August – 2 September 1994.

Manuscript was received on 28 October 1994, in final form 2 May 1995.